

The Science of Hardness Testing and Its Research Applications

Based on papers presented
at a symposium of the
American Society for Metals
October 18 to 20, 1971

Edited by
J. H. WESTBROOK and
H. CONRAD



AMERICAN SOCIETY FOR METALS
Metals Park, Ohio

Chapter 29

Environmental Effects in the Hertzian Test

B. R. LAWN

The status of the Hertzian indentation test as a means for investigating the fracture properties of highly brittle materials has grown rapidly during the past two decades. In this test, a hard sphere is loaded onto the surface of a specimen until a cone-shaped fracture initiates around the contact circle beneath the indenter (1). A theoretical understanding of cone-crack formation requires a fracture-mechanics analysis, taking into account the energetics of the cone as it propagates downward through the complex Hertzian stress field (2 to 7). In a microscopic picture of brittle fracture, it is convenient to regard crack growth as a bond-rupture process (the most brittle solids being covalently bonded) in which the work to fracture may be identified with the energy of the cohesive bond. This approach is particularly suited to a description of the rate-dependent effects that occur when an environmental species enters the crack and interacts with the crack-tip bonds. A detailed analysis of the mechanics of crack growth in these terms accordingly provides the basis for an experimental study of the controlling parameters of brittle fracture. In this light, the Hertzian test presents itself as a versatile fracture tool, at the same time retaining all the advantageous features of general indentation techniques.

In this paper, we outline the basic mechanics of the Hertzian test, with particular reference to the effects of a gaseous environment on the kinetics of cone-crack growth. Glass is chosen as a material for study because it is readily available in the slab-like form best suited to indentation testing, and because it is mechanically isotropic, thus making theoretical treatment of the deformation processes more viable: the applicability of the Hertzian method to the study of brittle solids in general is nevertheless stressed (3).

The author is at the School of Physics, University of New South Wales, Kensington, N.S.W., Australia.

Fracture Mechanics

General Formulation. The physical basis of present-day fracture mechanics derives from the energy-balance concept of Griffith (8). In an ideally brittle solid, the conditions of mechanical equilibrium require a balance between the strain energy released and the work done in overcoming interatomic cohesion at the crack tip as new fracture surface is created. This condition may be stated formally, for a crack of length c (Fig. 1), as

$$G_c = 2\gamma = N_A U_B \quad (\text{critical}) \quad (1)$$

where $G = -\partial U / \partial c$ is the strain-energy release rate, or crack-extension force, 2γ is the surface-tension force associated with the work required to rupture N_A bonds per unit area in creating two new surfaces, and U_B is the bond energy. Both G and γ are generally expressed as line forces per unit width of crack front.

A nonequilibrium crack system may exist in one of two states;

$$\begin{aligned} G &> G_c && (\text{supercritical}) \\ G &< G_c && (\text{subcritical}) \end{aligned} \quad (2)$$

In the supercritical state, the crack "runs" and the mechanics of crack propagation involves the kinetic energy of the material bounded by the separating crack walls. In the subcritical state, a brittle crack ideally should close up and heal along its interface, but in practice it is prevented from doing so by irreversible processes (9). In fact, the very agents which act to prevent healing are often responsible for subcritical crack extension. A discussion of nonequilibrium crack

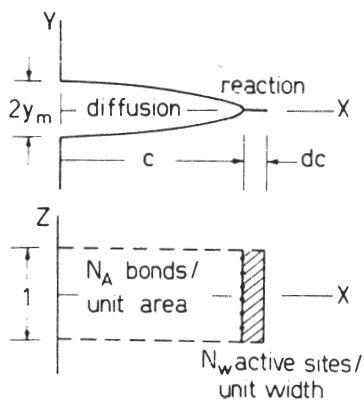


Fig. 1. Coordinate system for crack. Environmental species may enter crack mouth, diffuse along interface, and react with crack-tip bonds.

growth generally introduces kinetic terms into the problem. In terms of an atomistic process at the crack tip, we note that $dN = N_A dc$ bonds per unit width of front are ruptured in an incremental extension dc , so that the crack velocity may be written

$$v_c = \frac{dc}{dt} = \frac{1}{N_A} \frac{dN}{dt} \quad (3)$$

The rate of bond rupture may, in an environmental interaction, be controlled by the rate of chemical reaction at the tip, or rate of diffusion down the interface (Fig. 1). Typically, crack velocities in the supercritical region exceed those in the subcritical region by several orders of magnitude.

Mechanics of Cone-Crack Growth. In applying the principles of fracture mechanics to the cone-crack system, one makes use of the Hertzian elastic contact equations (1), which hold up to the point of fracture. Figure 2 shows the essential parameters. The indentation is geometrically similar for all sphere sizes if stresses are normalized to the mean indentation pressure

$$P_o = \frac{P}{\pi a^2}$$

and linear dimensions normalized to contact radius

$$a = \left(\frac{4k}{3E} Pr \right)^{1/3}$$

where P is the indentation load, r the sphere radius, E Young's modulus of the specimen material, and k a dimensionless constant (about equal to unity) in elastic terms.

The treatment assumes the crack to initiate from a surface flaw

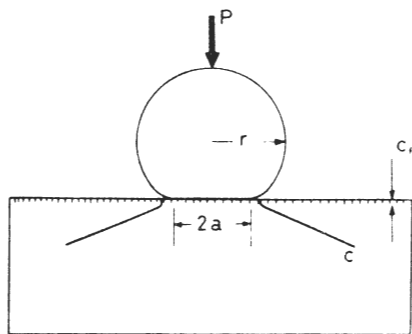


Fig. 2. Geometry of Hertzian test. Surface ring initiates from surface flaw, and propagates into full cone crack at critical indenter load.

of depth c_f in the vicinity of the contact circle, and to propagate downward as a surface ring. This assumption has both theoretical (3) and experimental (6) justification. For a cone crack of length c measured along the downward crack-path coordinate, x , the crack-extension force may be written (2-4)

$$G = \frac{P}{r} \left\{ \frac{3(1-\nu^2)}{\pi^3 k} \left(\frac{c}{a} \right) \left[\int_0^{c/a} \frac{[\sigma(x/a)/P_0] d(x/a)}{(c^2/a^2 - x^2/a^2)^{1/2}} \right]^2 \right\}$$

$$= \frac{P}{r} \phi \left(\frac{c}{a}, \text{elastic constants} \right) \quad (4)$$

Here $\sigma(x/a)$ is the tensile-stress distribution along the ultimate crack path prior to fracture, and ν is the Poisson's ratio of the specimen.

The function ϕ in equation 4 is evaluated in piecewise manner for increasing c by computer (3). Figure 3 shows the resulting crack-extension force, normalized to G_c , as a function of c/a . For a given indenter size, the curves scale with P . The curve labeled P_0^* , with its minimum at $G = G_c$, has special significance, as we shall see below, and all variables evaluated at P_0^* will be denoted by asterisk. The "hump" in the curves has its origin in the highly inhomogeneous nature of the Hertzian stress field (2, 6). Below the horizontal broken line in Fig. 3, the cone crack is subcritical; above

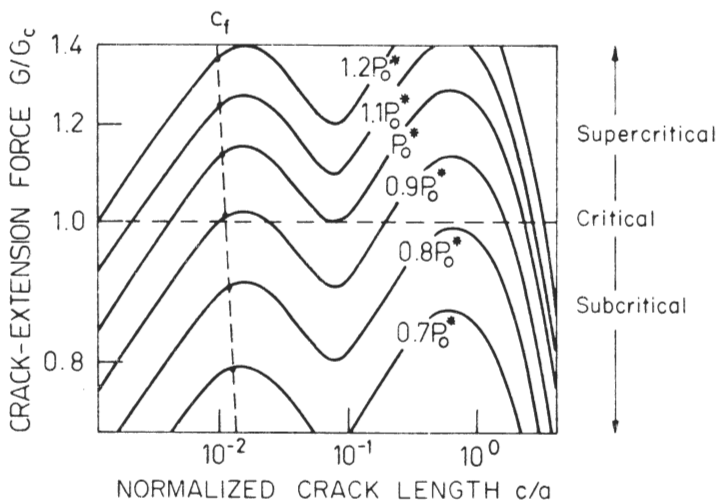


Fig. 3. Crack-extension force as function of cone-crack length. The curves scale with indenter load. The horizontal broken line represents Griffith equilibrium, and the near-vertical broken line represents the size of surface flaws. Curves computed for $\nu = 1/3$.

the line, it is supercritical. The near-vertical broken line connects points on successive curves at $c_f = \text{constant}$.

Environment-Free Conditions. Under environment-free conditions (for example, vacuum, temperatures approaching absolute zero), it is found that crack extension occurs only for $G \geq G_c$. We consider the manner in which a cone crack develops from a surface flaw in Fig. 4 (2-4). The flaw cannot initiate into a downward-propagating ring until $P = P_2$ in the figure. At that load, the flaw enters the supercritical region and grows spontaneously along the constant P_2 curve from the c_0 to the c_1 branch. For the ring to extend further to the c_2 branch, in the absence of any subcritical growth, the indenter load must be increased to $P = P_o^*$, where c_1 and c_2 merge at c^* , whereupon the ring grows supercritically into the full cone, from c^* to c_3^* . Typically, $c^* \approx 50 \mu\text{m}$, $c_3^* \approx 500 \mu\text{m}$ (6). It is this final unstable stage which is generally observable in a Hertzian test, and the critical condition for its occurrence is $P = P_o^*$, $c = c^*$, that is, from equation 4

$$G_c = \frac{P_o^*}{r} \phi \left(\frac{c^*}{a}, \text{elastic constants} \right)$$

which, combined with equation 1, gives the critical load

$$P_c = P_o^* = K(E) \gamma r \quad (5)$$

$\phi(c^*/a)$ may be evaluated from equation 4. This result, which holds for all $c_o^* \leq c_f \leq c^*$, and is independent of the original flaw size, c_f , expresses Auerbach's law (2). It may be of use in obtaining a measure of the fracture surface energy, γ .

Environment-Dependent Conditions. In the presence of an interacting environment, cone cracks may grow subcritically (10, 11, 5, 6). Suppose that we load the indenter to some value $P = P_1 < P_o^*$ as in Fig. 5, and maintain this level for a test duration t_D . We assume that the surface ring first extends spontaneously to the c_1 branch of the P_1 curve before the environment has time to interact with the crack tip. The ring is then free to grow subcritically from c_1 to c_2 , and thence into the full cone at c_3 , as shown in Fig. 5. If the rate-controlling process during this stage is stress enhanced (12), the crack velocity will be a function of G , hence of c (equation 4), and we may integrate equation 3 to obtain cone-crack length as a function of indentation time:

$$t_D = \int_{c_f}^c \frac{dc}{v_c(c)} \quad (6)$$

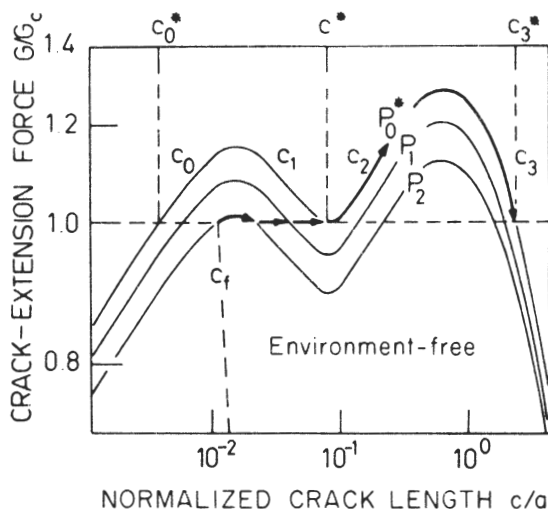


Fig. 4. Crack extension for environment-free conditions. No subcritical growth is permitted. Heavy, arrowed lines indicate stages of crack extension.

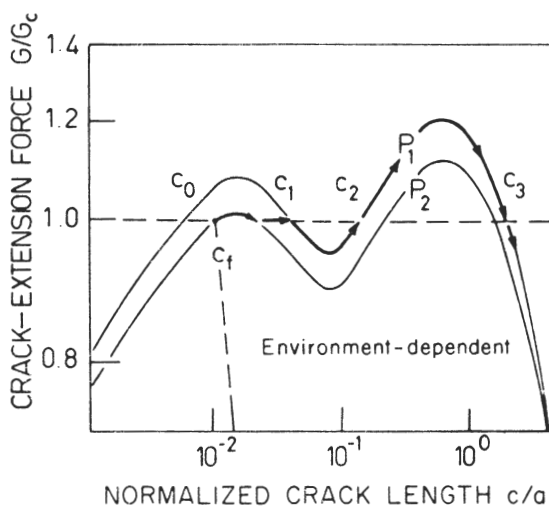


Fig. 5. Crack extension for environment-dependent conditions. The environmental interaction permits subcritical growth. Heavy lines indicate stages of crack extension.

In evaluating equation 6, we may neglect the relatively short times spent in supercritical growth. Thus, the time to full cone fracture is determined with c_1 and c_2 as limits.

The integration in equation 6 may, in principle, be computed piecewise with increasing c , simultaneously with that in equation 4. However, detailed knowledge of the interaction mechanism is required before $v_c(c)$ can be specified.

Experimental

Apparatus. The cone-crack experiments are carried out within an environmental test chamber (13) (Fig. 6). An external load is transmitted to the indenter, a 1/2-in.-diam. tungsten carbide sphere, via a vertically flexible bellows system. The load delivered to the specimen is measured by means of an internal load cell. Facility exists for evacuating the system (10^{-6} torr), for heating the specimen (500 C), and for admitting a gas or liquid environment to the specimen. Over a hundred tests can be performed on one specimen surface 2 by 2 in., with external control of indentation site.

For all runs on 1/2-in.-thick glass slabs, a standard pretest abrasion treatment in a slurry of grade 400 SiC powder ensures a uniform

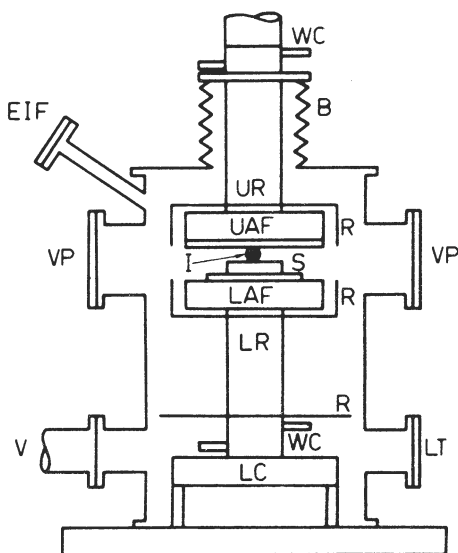


Fig. 6. Environmental chamber for Hertzian fracture testing. B, bellows; UR, upper ram; LR, lower ram; UAF, upper anvil-furnace assembly; LAF, lower anvil-furnace assembly; S, specimen; I, indenter; LC, load cell; VP, viewing ports; EIF, environment-inlet flange; V, vacuum connection; LT, lead-through flange; R, reflector plates; WC, water cooling.

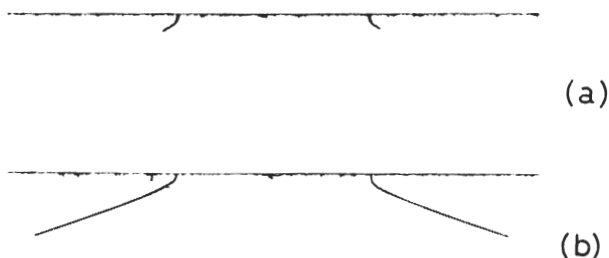


Fig. 7. Etched sections of cone-crack profiles. (a) Surface ring, (b) fully developed cone. Width of surface ring, 860 μm .

distribution of surface microcracks within the size range $c_o^* \leq c_f \leq c^*$ indicated in Fig. 4 (4). In vacuum, full development of the Hertzian cone is observed visually, through viewing ports in the chamber walls, at a critical load $P_c = P_o^* \approx 100$ kg. This value sets the scale of loads for the sequence of curves of Fig. 3.

Tests in the presence of a reactive environment are more difficult to monitor. The small scale of the fracture to $c = c_2$ rules out detailed optical measurement of crack growth with indentation time. It is necessary under such conditions to resort to indirect methods, such as a section-and-etch examination of the specimen after indentation (6). With this method, a series of indents, systematically varied with indentation load and time, is made along a straight line in the specimen surface. A section and polish down to the plane bisecting the indentations, followed by a light etch in dilute HF, then reveals the cone-crack profiles. Figure 7 illustrates two such profiles, the first showing the surface ring arrested during subcritical growth between the c_1 and c_2 branches of Fig. 5, and the second showing the full cone at c_3 .

Tests in Air. The results of a section-and-etch study of cone-crack growth in laboratory atmosphere, at $P = 65$ kg, are shown in Fig. 8. The subcritical stages between c_1 and c_2 , and along c_3 , are readily identified as the regions of relatively slow growth. There is considerable uncertainty associated with the data for $t_D < 1$ sec(s), and $c \approx c_f$, owing to experimental limitations (6). Thus, the data in Fig. 8 are not considered sufficiently accurate for determining instantaneous crack velocities, v_c , in subcritical growth to c_2 , although they are adequate for estimating the mean velocity, v_m ; we obtain $v_m \approx 7 \times 10^{-5}$ msec $^{-1}$ from the figure. Tests in liquid environments show crack-growth curves similar to that of Fig. 8, but with different rates of propagation (6).

The manner in which v_m varies with indenter load for tests in air is shown in Fig. 9. Errors become more serious as P_o^* is approached, the rings propagating more rapidly through the diminishing hump region (Fig. 5). Nevertheless, the tendency for the velocity to increase with applied loading, and to saturate at a value of 10^{-3} to 10^{-4} msec $^{-1}$,

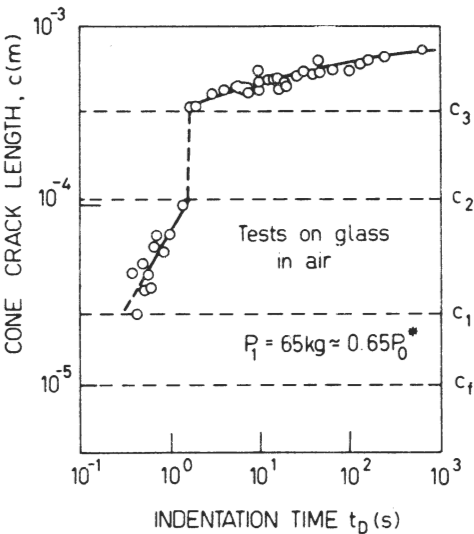


Fig. 8. Cone-crack length as function of indentation time. Section-and-etch data. Uncontrolled atmosphere, relative humidity \approx 30%.

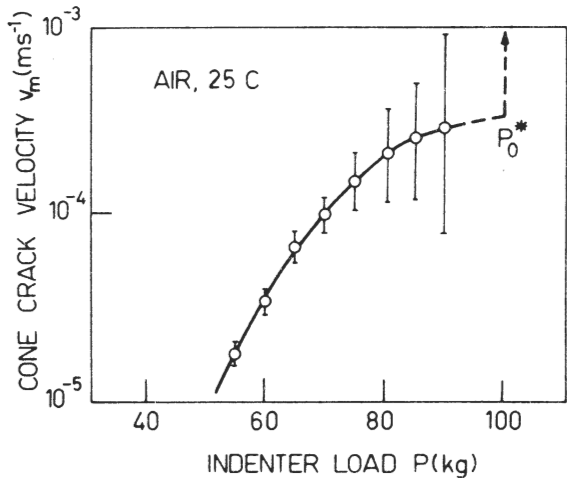


Fig. 9. Mean crack velocity for subcritical growth between c_1 and c_2 branches, as function of indenter load.

appears to be real. The same trend has been observed by Wiederhorn (14) and Schönert *et al.* (15) for cleavage tests on glass slides in moderately humid atmospheres.

Environmental Interaction

Chemical Interaction as a Two-Stage Process. The type of behavior observed in Fig. 9 can be explained in terms of a two-stage kinetic process (14). First, because of the fine scale of the crack-wall separation, we might expect diffusion processes to control the flow rate of environmental species to the crack tip. Second, we might expect the rate of the ensuing chemical reaction at the tip to control the rate at which bonds are ruptured. Whichever of the two stages is slower would limit the overall rate of crack growth. The reaction is generally described as an activated process, in which n molecules of gas react with a crack-tip bond to form an activated complex, and thereby lead to rupture;



where n is the order of the reaction. Under steady-state conditions, the bond-rupture rate dN/dt is related to the molecular flow rate dM/dt to the tip by

$$\frac{dN}{dt} = \frac{1}{n} \frac{dM}{dt} \quad (8)$$

The application of a stress is taken to lower the activation energy for the reaction, thus accounting for the increase in crack velocity with load. The diffusion step, on the other hand, is unlikely to be greatly affected by applied load, and this would explain the plateau in the curve as the critical condition (equation 1) is approached.

Diffusion of a Dilute Gas. There are several possible modes in which reactive molecules may diffuse to the crack tip. For instance, transport may occur by surface diffusion along the crack walls, or by diffusion through a dense phase (that is, intermolecular spacing \ll crack-wall separation) of gas, liquid or solid (corrosion product) along the crack interface (14). In each of these cases, the transport mechanism can be characterized by a diffusion coefficient which is insensitive to crack geometry. For a dilute (Knudsen, ref 16) gas, however, molecule-to-wall collisions determine the flow through narrow channels ("free-molecular flow"), and the diffusion coefficient becomes a function of the crack-wall separation. In our experiments, the mouth opening of the fully developed cone is $2y_m \approx 1 \mu\text{m}$ (Fig.

1) under load (9), so that the crack-wall separation in the prior subcritical stage of growth might be expected to compare with the mean free path, $\approx 0.1 \mu\text{m}$, of molecule-to-molecule collisions in air at standard temperature and pressure. Under such conditions, we may assume the gaseous environment to be dilute, and this assumption will hold to better approximation as the molecules diffuse along the narrowing interface toward the crack tip, and as the pressure in the test chamber is reduced.

The steady-state flow rate of molecules to the crack tip is determined by the difference in partial pressure, $p_m - p_c$, between mouth (source) and tip (sink) of the reacting species. The free-molecular-flow equation may be written (17)

$$\frac{dM}{dt} = \frac{2y_m A}{(2\pi mkT)^{1/2}} (p_m - p_c) \quad (9)$$

where m is the mass of the reactive molecule, k is Boltzmann's constant, T is absolute temperature, and A is an "attenuation" factor, always less than unity, representing the ratio between the rate at which molecules arrive at the tip and that at which molecules enter the mouth. dM/dt increases as p_c decreases, which obtains when the rate of chemical reaction becomes high. Equations 3, 8 and 9 may then be combined to give

$$v_c = v_d (1 - p_c/p_m) \quad (10)$$

where, in the limit of an "instantaneous" reaction ($p_c \rightarrow 0$),

$$v_d = \frac{2y_m A p_m}{nN_A (2\pi mkT)^{1/2}} \quad (11)$$

represents the maximum attainable crack velocity. We note that equation 11 contains only parameters of the diffusion process, that is, the crack growth is diffusion controlled.

It is of interest to evaluate v_d for the conditions of the present experiments, assuming one molecule of water vapor to react with one Si-O bond in the glass. We take $n = 1$, $N_A = 3.5 \times 10^{18}$ bonds m^{-2} (glass), $m = 3.0 \times 10^{-26}$ kg (H_2O), $T = 300$ K, $2y_m \approx 1 \times 10^{-7}$ m, $p_m = 3 \times 10^3$ Nm^{-2} (100% RH), giving $v_d \approx 3A$ msec^{-1} . The attenuation factor is more difficult to specify. If the crack interface is approximated to a rectangular channel (18), of section $c \times 2y_m$, we obtain for $c \approx 1 \times 10^{-4}$ m the value $A \approx 3 \times 10^{-3}$, which gives $v_d \approx 1 \times 10^{-2}$ msec^{-1} . This result is likely to be an overestimate, since we have taken the extreme cases of a saturated atmosphere

and a crack of nondiminishing cross section. The calculation may, therefore, be regarded as giving at best an order-of-magnitude prediction of the limiting velocity at the plateau in Fig. 9.

Reaction Kinetics. As the reactive molecules rupture the crack-tip bonds, the crack advances, leaving the adsorbed products behind on the newly created surfaces. The rate of bond rupture may, for an activated process, be written

$$\frac{dN}{dt} = N_w K \quad (12)$$

with N_w the number of active bond sites per unit width along the crack front, and K the rate of reaction for one bond. From the theory of absolute reaction rates (19), we obtain

$$K = \frac{kT}{h} \left\{ \exp \left(- \frac{\Delta F_r^*}{kT} \right) - \exp \left(- \frac{\Delta F_p^*}{kT} \right) \right\} \quad (13)$$

where h is Planck's constant, ΔF_r^* and ΔF_p^* are the free energies of formation of the activated complex from reactants and products, respectively. Assuming $\Delta F_r^* \ll \Delta F_p^*$, we require knowledge of the dependence of ΔF_r^* on such variables as T , G , p_c for a detailed description of the reaction process.

Wiederhorn (14), following a procedure developed by Charles and Hillig (12) for a stress-corrosion mechanism, derives a relation for a gaseous environment which we may write in the form

$$K = C(T) p_c^n \exp \left[\frac{-E_B^* + f(G)}{kT} \right] \quad (14)$$

where $C(T)$ is a (slowly varying) temperature-dependent term, E_B^* is an activation energy, and $f(G)$ is a monotonic function of crack-extension force representing the free energy reduction arising from an applied load. Combining equation 14 with equations 3 and 12, and eliminating p_c from equation 10, we obtain the following implicit equation in v_c

$$v_c = v_d \left\{ 1 - \left(\frac{v_c}{v_{ro}} \right)^{1/n} \exp \left[- \frac{f(G)}{nkT} \right] \right\} \quad (15)$$

where we have written

$$v_{ro} = \frac{N_w}{N_A} C(T) p_m^n \exp \left(- \frac{E_B^*}{kT} \right) \quad (16)$$

At low loads, the second term within the brace in equation 15 approaches unity, and the crack velocity is in the limit

$$v_r = v_{ro} \exp \left[\frac{f(G)}{kT} \right] \quad (17)$$

We note that equation 17 involves only parameters of the chemical reaction, that is, the diffusion is effectively instantaneous, and the crack growth is reaction controlled. The appearance of the exponential term is consistent with the behavior of the curve in Fig. 9 in the lower load range.

Concluding Remarks

Ideally, a rigorous test of the foregoing theory would involve a generation of crack-growth curves, by insertion of equation 15 into equation 6, to match such data as shown in Fig. 8. However, this would involve a deeper consideration of the reaction mechanism than we have given here. Moreover, there exist quantitative discrepancies between the theoretically predicted and experimentally observed fracture-mechanics function $G(c/a)$ for cone cracks (6), and until these are resolved, there appears to be little chance of accurately describing kinetic effects. On the other hand, investigations into the pressure and temperature dependence of the crack-velocity equations, particularly in the limiting regions (equations 11, and 16 and 17), should test the essential framework of the theory, and provide values for activation energies and other parameters. The Hertzian test thereby offers a simple means for rapid accumulation of fracture data relating to such strength-controlling properties as fracture surface energy and rates of chemical reaction.

Acknowledgment. The author is grateful to J. E. Sinclair for discussions. Some of the results presented here are by courtesy of J. J. H. Beek (Fig. 6) and A. G. Mikosza (Fig. 7 to 9).

References

- 1 H. Hertz, Hertz's Miscellaneous Papers, Macmillan, London, 1896, Chapters 5 and 6.
- 2 F. C. Frank and B. R. Lawn, Proc Roy Soc, **A299**, 291 (1967).
- 3 B. R. Lawn, J Appl Phys, **39**, 4828 (1968).
- 4 F. B. Langitan and B. R. Lawn, J Appl Phys, **40**, 4009 (1969).
- 5 F. B. Langitan and B. R. Lawn, J Appl Phys, **41**, 3357 (1970).
- 6 A. G. Mikosza and B. R. Lawn, J Appl Phys, **42**, 5540 (1971).

- 7 T. R. Wilshaw, The Hertzian Fracture Test, Sussex University Report No. 70/Mat/21, 1970.
- 8 A. A. Griffith, Phil Trans, **A221**, 163 (1920).
- 9 J. S. Williams, B. R. Lawn, and M. V. Swain, Phys Status Solidi (a), **2**, 7 (1970).
- 10 F. C. Roesler, Proc Phys Soc (London), **B69**, 55, 981 (1956).
- 11 C. J. Culf, J Soc Glass Technol, **41**, 157 (1957).
- 12 R. J. Charles and W. B. Hillig, Symposium on Mechanical Strength of Glass and Ways of Improving It, 1961, p 511.
- 13 J. J. H. Beek and B. R. Lawn, J Phys E: Sci Instrum, **5**, 710 (1972).
- 14 S. M. Wiederhorn, J Amer Ceram Soc, **50**, 407 (1967); Mechanical and Thermal Properties of Ceramics, J. B. Wachtman Jr., editor, NBS Special Publications No. 303, 1969, p 217.
- 15 K. Schönert, H. Unchauer, and W. Klemm, Second Intern Conf Fracture, Brighton, 1969, paper 41.
- 16 M. Knudsen, The Kinetic Theory of Gases, Methuen, London, 1950.
- 17 S. Dushman, Scientific Foundations of Vacuum Technique, John Wiley, New York, 1962.
- 18 K. U. Snowden, Acta Met, **12**, 295 (1964).
- 19 S. Glasstone, K. J. Laidler, and H. Eyring, Theory of Rate Processes, McGraw-Hill, New York, 1941.
- 20 G. R. Irwin, Handbuch Physik, Springer, Berlin, 1958, p 551.